

2019:01239- Unrestricted

# Report

## Characterization of inclusion content in mechanical aluminium filters

### Author

Ulrik Aalborg Eriksen, Inge Johansen, Martin Syvertsen, Anne Kvithyld, Sarina Bao





# Report

## Characterization of inclusion content in mechanical aluminium filters

**KEYWORDS:**  
Aluminium, inclusions,  
filtration, BPF, CFF

**VERSION**  
Version 02

**DATE**  
2019-07-19

**AUTHOR(S)**  
Ulrik Aalborg Eriksen, Inge Johansen, Martin Syvertsen, Anne Kvithyld, Sarina Bao

**CLIENT(S)**  
BEST Project

**CLIENT'S REF.**  
Steering committee BEST

**PROJECT NO.**  
102015501

**NUMBER OF PAGES/APPENDICES:**  
14/2

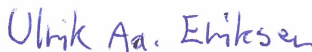
### ABSTRACT

#### Characterization of mechanical filter performance

Bonded particle and ceramic foam filters used in filtration experiments of an AA608250 alloy at Sunndalsøra May 2019 have been studied under the light microscope. Pictures taken have been digitally analysed to characterize the inclusion content in the spent filters. It was found that for melts with low cleanliness, the distribution in the filters is exponential. Both filter types capture a high number of inclusions at the inlet, but the BPFs capture more particles deeper into the filter.

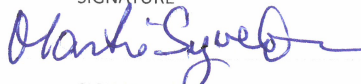
**PREPARED BY**  
Ulrik Aalborg Eriksen

SIGNATURE



**CHECKED BY**  
Martin Syvertsen

SIGNATURE



**APPROVED BY**  
Morten Onsjøien

SIGNATURE



**REPORT NO.** 2019:01239  
**ISBN** 978-82-14-06250-2

**CLASSIFICATION**  
Unrestricted

**CLASSIFICATION THIS PAGE**  
Unrestricted

# Document history

---

<b>VERSION</b>	<b>DATE</b>	<b>VERSION DESCRIPTION</b>
Version 01	2019-11-09	Final version

# Table of contents

<b>1</b>	<b>Introduction .....</b>	<b>5</b>
<b>2</b>	<b>Experimental.....</b>	<b>5</b>
<b>3</b>	<b>Results and discussion .....</b>	<b>6</b>
3.1	LiMCA results and pressure drop.....	6
3.2	Inclusion distribution in the filters.....	7
3.3	Size distribution of inclusions .....	9
3.4	Other findings .....	10
<b>4</b>	<b>Conclusion.....</b>	<b>11</b>
<b>5</b>	<b>Further work .....</b>	<b>11</b>
<b>6</b>	<b>References .....</b>	<b>12</b>
<b>A</b>	<b>Appendix.....</b>	<b>12</b>
A.1	Pressure drop.....	12
A.2	The trapezoidal rule .....	13

## APPENDICES

---

A.1 Pressure drop  
A.2 The trapezoidal rule

---



## 1 Introduction

The removal of inclusions from molten aluminium is essential to assure the quality of the final products. Capturing the inclusions in a mechanical filter is a common method to increase the purity of the alloy. Bonded particle filters (BPF) and ceramic foam filters (CFF), both with varying porosity, were used in filtration experiments performed at Sunndalsøra during the 19<sup>th</sup> week of 2019.

The purpose of this work is to characterize the inclusion content in the spent filters. Inclusions will be mapped using the optical light microscope and counted using digital image analysis. These findings will be compared to other melt analyses, including the in-line LiMCA results. Understanding the inner workings of the filters will make it possible to optimize the refining process, both with respect to product quality and costs. There are mainly two proposed mechanisms for filtration – cake and depth filtration as sketched in figure 1 [1]. The distribution of inclusions in the filters might provide some insight into the contribution of each mechanism to the overall inclusion capture.

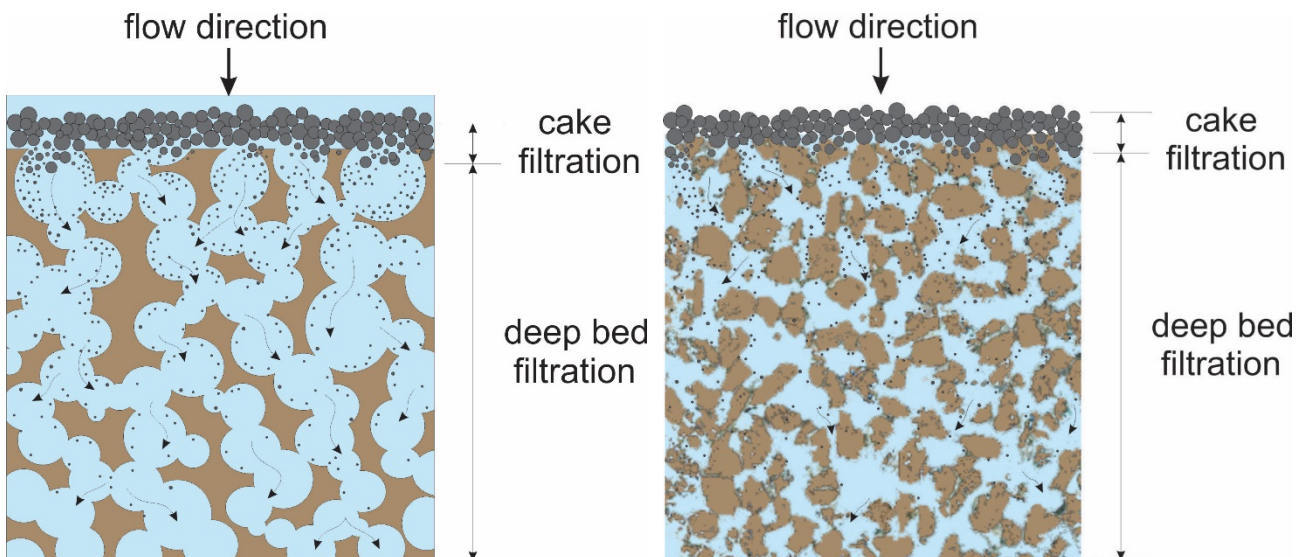


**Figure 1: Sketches illustrating filtration in a CFF and BPF respectively. Schematics by Arjan Cifja.**

## 2 Experimental

In total, eight filters were tested in filtration experiments at Sunndalsøra, four of which were BPFs and the other four CFFs. Three of each were chosen to be studied under the light microscope. The BPFs were of grit sizes of 10 and 14 and CFFs of grades 65 and 80. According to the producer, the 10 and 14 grits correspond to the 65 and 80 grades respectively. The melt chemistry was roughly the same each day, close to the AA608250 alloy, though with some variation in inclusion content. This difference in inclusion content was measured by LiMCA. LiMCA #1 and #2 were placed upstream and downstream of the filter respectively, making it possible to measure the efficiency of the filters. In addition, PoDFA samples were taken and pressure drop over the filter measured.

In the light microscope 8x4 pictures (each of resolution 3840x2400) were analysed, which with a 50x total magnification corresponds to slightly more than 70% of the cross section mapped at each filter depth. Each

picture was divided into three in the direction of metal flow, to get better depth-resolved data. This is important because the inclusion concentration in the filter can, as previously seen, change rapidly the first few millimetres [2]. The BPF and CFF filters are approximately 25 and 50 mm thick respectively. Only the first 5 mm were studied in both cases.

Counting inclusions in the filters is challenging, mostly due to oxides occasionally being difficult to distinguish from filter chunks. When in doubt, these particles have been counted, meaning the results are likely to be a slight overestimate. For a detailed overview of the different particles imaged, see the previous work on inclusion counting [2].

The pictures were analysed using the ImageJ software. The threshold was manually set, inaccuracies were corrected for, and the area of all inclusions and filter pieces was recorded. This makes it possible to calculate both area fraction and the size distribution of the inclusions in the aluminium matrix.

### 3 Results and discussion

#### 3.1 LiMCA results and pressure drop

The initial inclusion content in the melt has a high impact on the number of particles captured in the filters. These concentrations were measured using the upstream LiMCA and are shown in table 1.

**Table 1: The initial LiMCA readings and steady state pressure drop for each experiment.**

Filter	Initial concentration [k/kg]	Pressure drop [mm]
Grit 10M	15	18
Grit 14Th	120	70
Grit 14F	100	79
Grade 65Tu	20	25
Grade 80Tu	18	20
Grade 80W	30	70

This difference in melt cleanliness is correlated to the difference in pressure drop. If a cake is formed at the inlet, the resistance in the filter will increase due to the smaller cross section available for metal flow. The particles making up the cake will therefore act as a filter to future incoming particles. The correlation between particles sizes, pressure drop, and efficiency is shown in figure 3. The elevated pressure drops for the two 14 Grits and the grade 80W filter might therefore indicate a cake formation. In the following image analysis, notable cake formations are found in all three filters. A snapshot of this cake taken in the light microscope of Grit 14F Edge can be seen in figure 2.

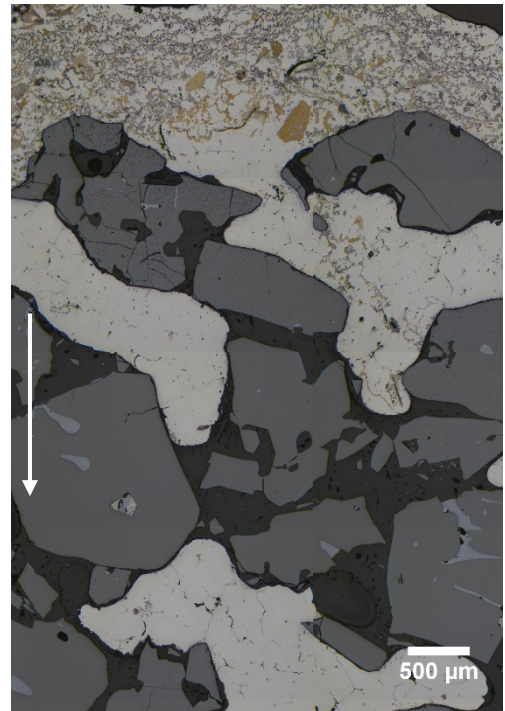


**Figure 2: A slice of the first few mm of Grit 14F edge. Arrow indicates direction of metal flow.**



### 3.2 Inclusion distribution in the filters

The area percentage of inclusions in the aluminium matrix was calculated for each individual picture taken. The following results are an average of all the pictures taken at the same depth. Only pictures with a minimum matrix area were included, as single particles get too high an impact if the measured matrix area is too small. For the BPFs this minimum requirement was set to 10 %; for the more porous CFFs the minimum was set to 25 % of the matrix area.

The distribution of inclusions in the filters was found to differ significantly between the filters with low and high pressure drop due to cake formation. Figure 4 shows the distribution for the filters with a high pressure drop. Most notably is it that the inclusion concentration is high near the inlet, and quickly stabilizes to a level under 5 % deeper into the filter. Also, it is worth noting that it seems like the CFFs stabilize more rapidly, and at a lower concentration level (below .5 %), than the BPFs. This implies that depth filtration contributes more to the overall filtration in the BPFs. A quantification of this difference in distribution is proposed in table 2, where the depth at which 90 % of the counted inclusions are captured is given for each sample. The trapezoidal rule was applied to estimate the area under the graph, essentially interpolating by linear regression between data points.

Another observation, which corroborates previous results [2], is that the filter geometry seems to affect distribution much more for the BPFs. This results in more inhomogeneous inclusion content for a given cross section, and less of a strictly decreasing concentration trend in the direction of current flow.

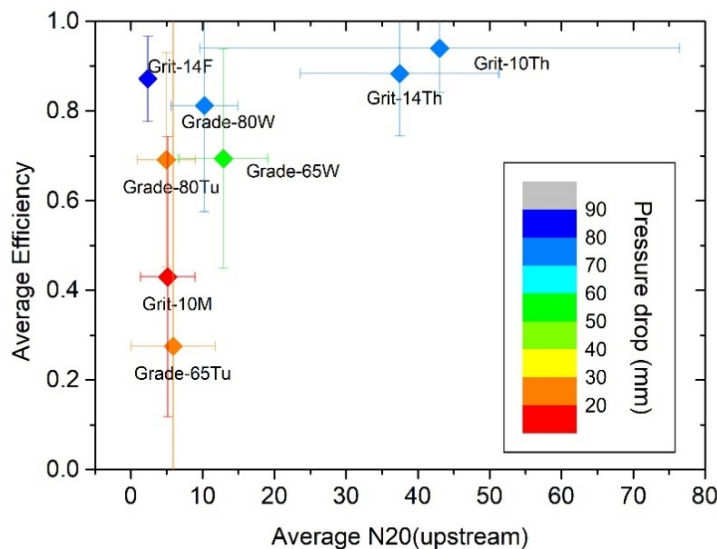
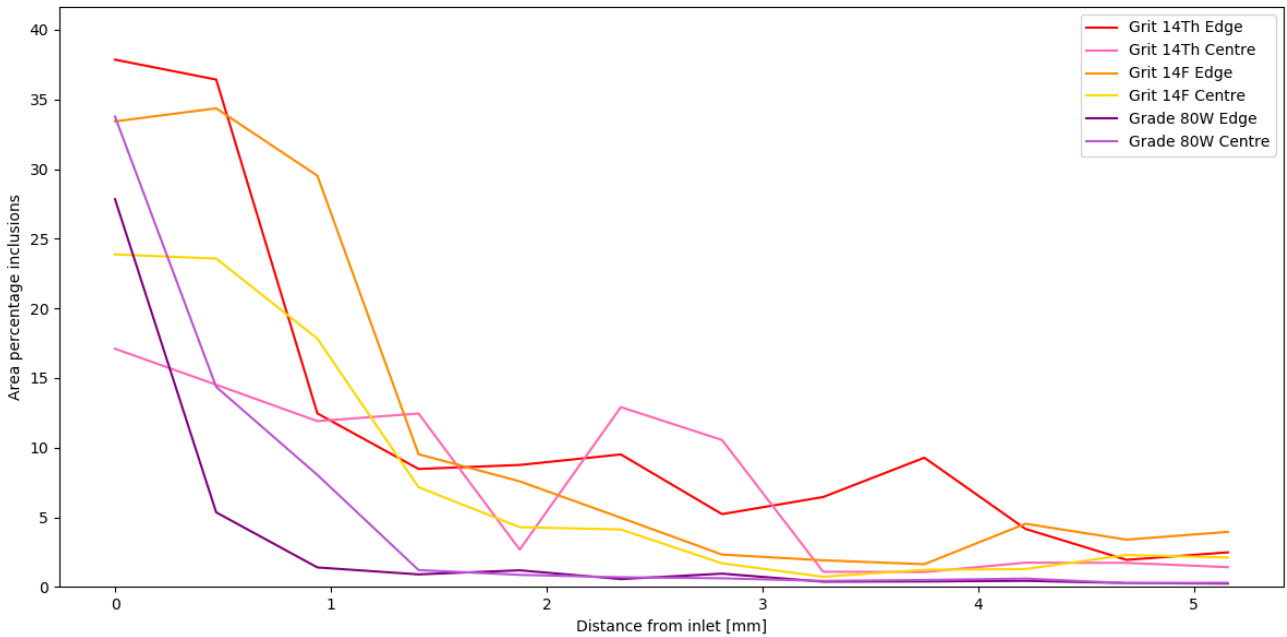


Table 2: The depth at which 90 % of the counted inclusions were captured.

Sample	90 % captured [mm]
BPF	3.24 (avg.)
Grit 14Th Edge	3.74
Grit 14Th Centre	3.01
Grit 14F Edge	3.45
Grit 14F Centre	2.75
CFF	2.05 (avg.)
Grade 80W Edge	2.56
Grade 80W Centre	1.54

Figure 3: Efficiency is calculated using upstream and downstream LiMCA N20 values. The efficiency increases with pressure drop.

The distribution of inclusions in the remaining filters are graphed in figure 5. For these filters, possibly apart from grade 65Tu Centre, there are no evident increase in concentration at the inlet. Instead, the concentration seems to be somewhat constant throughout. No obvious cake formation was observed for any of these filters in the light microscope either. Also, due to the overall low inclusion content, the measurements are more sensitive to the unavoidable counting errors.



**Figure 4: Percentage of inclusions in the aluminium matrix as function of distance from the inlet.**

For all the measurements there are seemingly a pattern where the edge of the BPFs and centre of CFFs captures the most inclusions. The difference is in several instances significant enough to be easily observable in the light microscope. The reason for this is unknown, but these results coincide with previous experiments with BPFs [2]. This could be an effect of the experimental setup, or even randomness due to limited sample size.

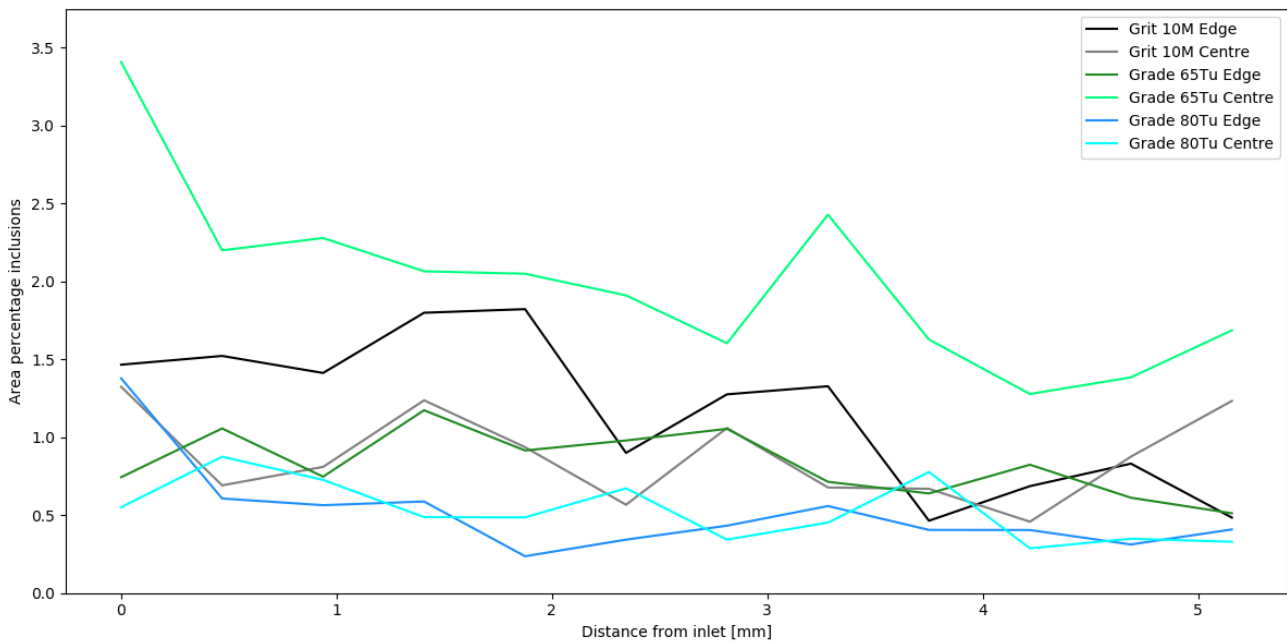


**Figure 5: Percentage of inclusions in the aluminium matrix as function of distance from the inlet.**

### 3.3 Size distribution of inclusions

The size distribution in the filters were calculated by counting the total number of inclusions in the size bin and dividing by the total photographed matrix area. All particles are imagined as circles to appoint a diameter.

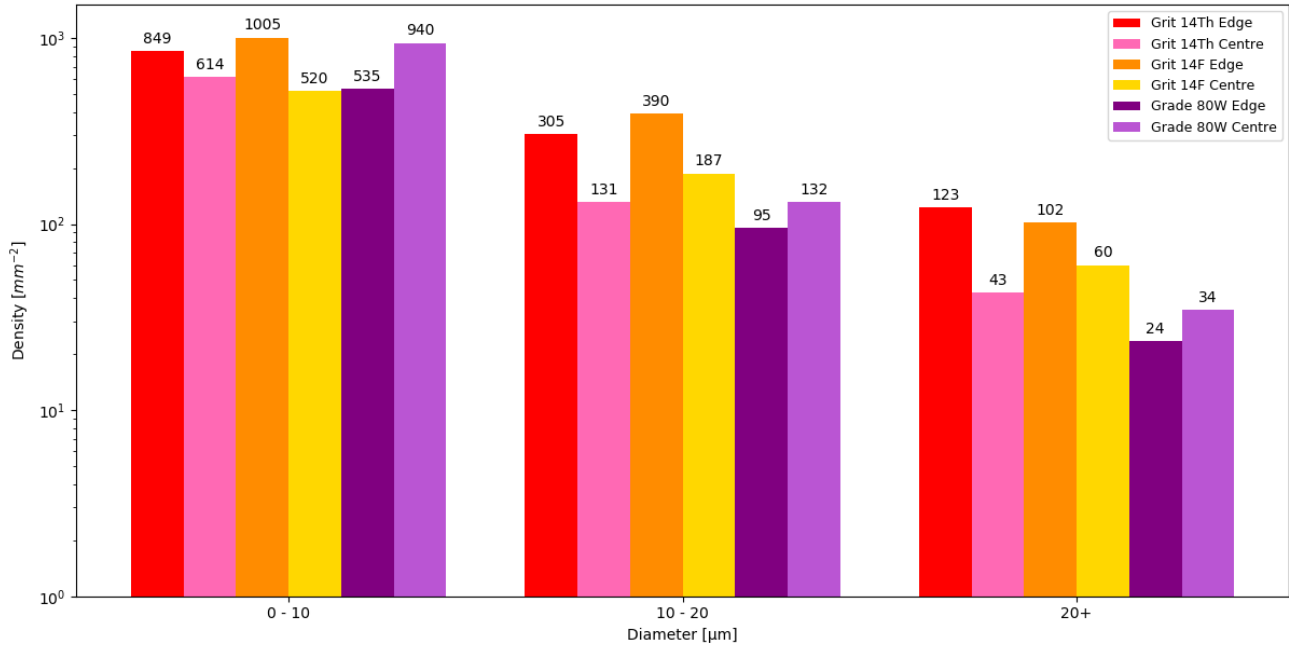


**Figure 6: Number of inclusions per matrix area for different size ranges.**

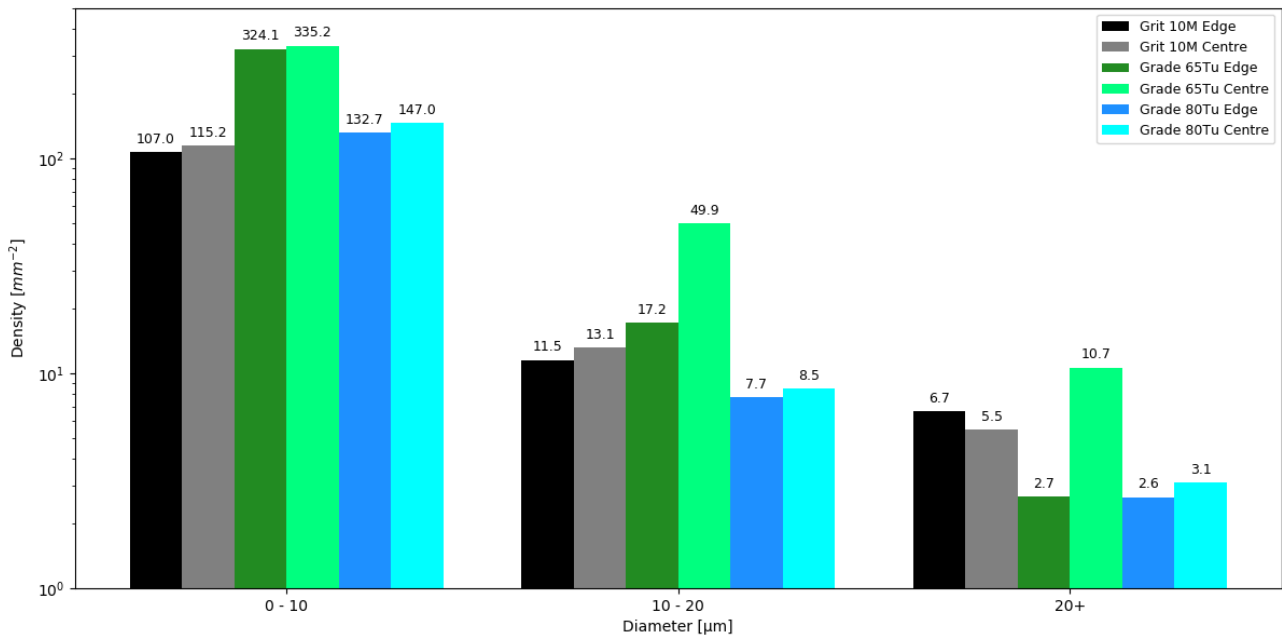


**Figure 7: Number of inclusions per matrix area for different size ranges.**

Figures 6 and 7 show the size distribution of inclusions for all the filters. Generally, the density seems to be around one order of magnitude higher for the samples in figure 6. These are the same filters which had a high pressure drop and cake formation. Grade 65Tu seems to be somewhat stuck in the middle, having both relatively high and low readings. Interestingly, this filter is capturing more than the denser grade 80Tu filter. This indicates that the small decrease in melt cleanliness, as shown in table 1, have a bigger impact on the capture rate than the increased porosity of the grade 65.

### 3.4 Other findings

An attempt was made to compare the expected number of particles captured in the filter from the LiMCA measurement to the results from the image analysis. This was done considering the difference between LiMCA #1 and LiMCA #2 N20 values, the mass flow rate through the filter and the filtration duration. Total number of inclusions captured and volume fraction of inclusions in the filter were calculated. No obvious correlations were discovered. This might potentially be due to variation in the accuracy of the available process data. However, it is not obvious that there necessarily must be a high correlation between the different measuring techniques. Most particles counted in the image analysis are smaller than the 20 microns particles which are counted by the in-line LiMCA.

It is worth mentioning that counting in the grade 80W filters was especially challenging. This is due to a brown layer surrounding the filter, as seen in figure 8. This layer was interfering with the image analysis software and demanded manual interventions. A possibility is that this filter has chemically reacted with the melt. The possible implications on filtration efficiency are unknown. Nothing like this was observed in any of the other examined filters.

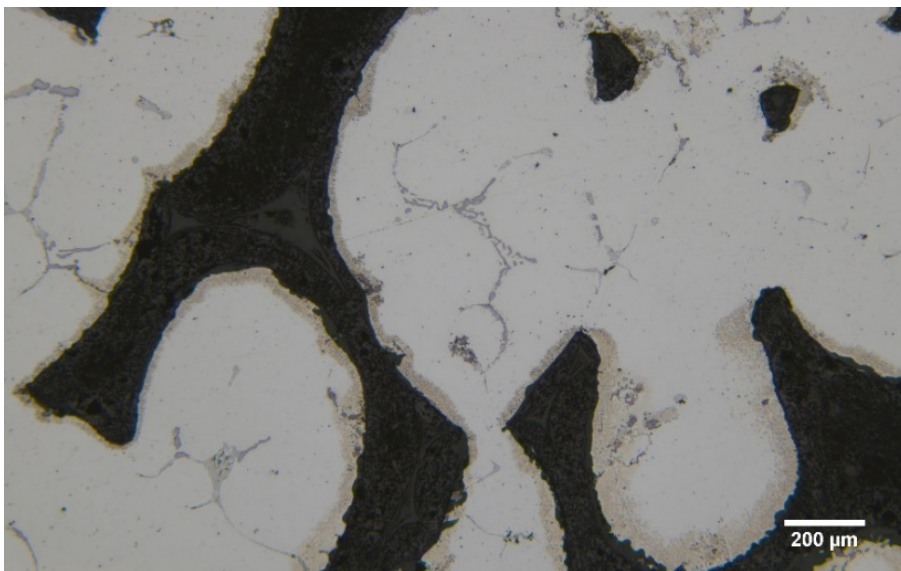


**Figure 8: The brown layer surrounding the black filter was only observed in the two Grade 80W samples.**

Upon inspection of the filters samples two months later there were obvious differences. This is likely due to oxidation of carbides after being exposed to atmospheric conditions, see figure 9. To ensure that measurements of inclusion content is comparable between samples, the samples should be polished before taking pictures. After oxidation, the area of inclusions measured will be noticeably larger.

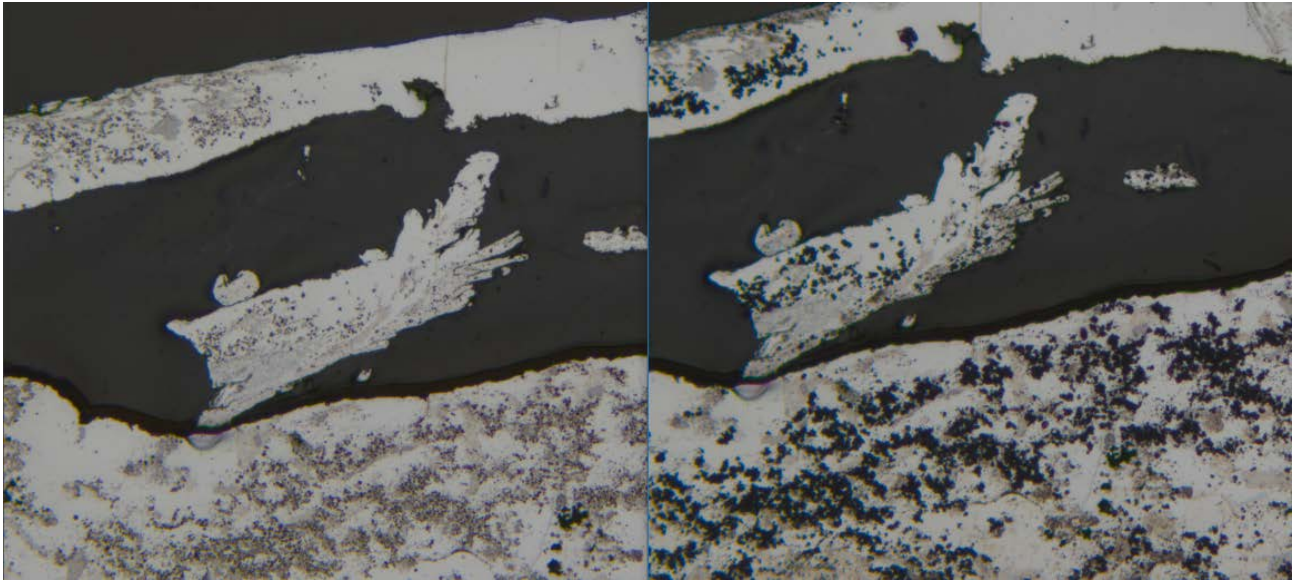


**Figure 9: The right picture was taken 2 months later than the left one. The sample was exposed to ambient conditions.**

## 4 Conclusion

The distribution of inclusions is rather constant throughout the filter for low inclusion concentrations, but shift to become close to exponentially distributed at higher concentrations. At the inlet, the two filter types capture comparable amounts of inclusions. The BPFs are showing higher capture rates further into the filter than the CFFs, suggesting that the contribution of depth filtration is higher for the former.

## 5 Further work

First and foremost, studying the effect of longer filtration times would be valuable. The BPFs need to have a higher capacity to be commercially viable due to their higher cost. It would be interesting to study how long the filters can be in use before they get clogged and must be replaced. Such an experiment might also reveal further information on potential difference in mechanism between the different filters.

Furthermore, it would be interesting to perform more experiments with high inclusion content to see if the results are consistent. More experiments might also shed some light on if there really is a systematic difference in performance between the edge and centre of the filters.

## 6 References

- [1] T. A. Engh, Principles of Metal Refining, New York: Oxford, 1992.  
 [2] U. A. Eriksen, "Inclusion counting in BPF-Filters," Sintef, Trondheim, 2018.

## A Appendix

### A.1 Pressure drop

Figure 10 graph the evolution of the pressure drop over the filter as a function of filtration time. For the grit 14Th filter the available data points are limited due to a malfunction, the filtration time was longer than the graph indicates. For the grade 80W the pump speed was adjusted, which is the reason for the dip to around 50 mm.

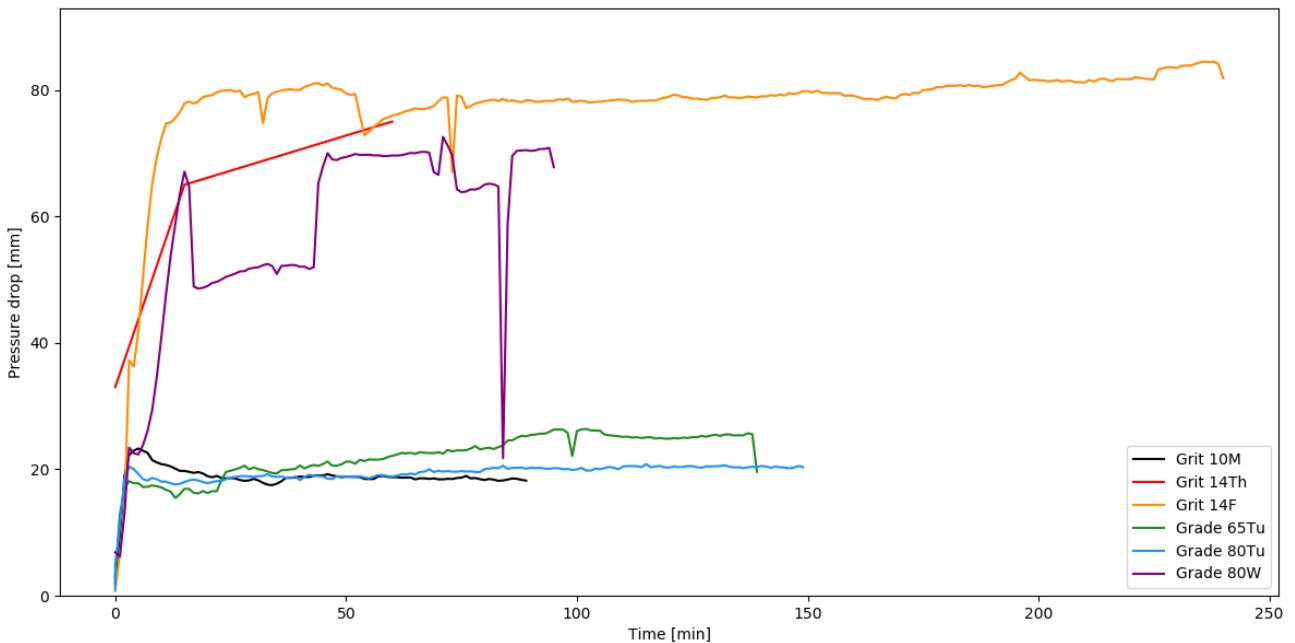


**Figure 10: The pressure drops during the filtration experiments. Grit 14<sup>th</sup> measurements were manually recorded.**

## A.2 The trapezoidal rule

The depth at which 90 % of inclusions were captured was calculated analytically using the trapezoidal rule. This can be expressed by the equation:

$$0.9 \times A_{Total} = \sum_{i=0}^n A_i - \frac{1}{2}(x_{n+1} - D) \times \left( 2 \times y_{n+1} - \frac{dy_n}{dx_n} \times D \right) \quad (A.1)$$

where  $A_{Total}$  is the total area under the graph,  $A_i$  is the area of each trapezoid, the  $n$  is the number of the last trapezoid which make the summed area exceed 90 % of the total. The solution is as follows:

$$D = \frac{1}{\frac{dy_n}{dx_n}} \left( \sqrt{-2 \times \sum_{i=0}^n A_i \times \frac{dy_n}{dx_n} + 1.8 \times \frac{dy_n}{dx_n} \times A_{Total} + y_{n+1}^2 + \frac{dy_n}{dx_n} \times x_{n+1} - y_{n+1}} \right) \quad (A.2)$$



Technology for a better society

[www.sintef.no](http://www.sintef.no)